SARS-CoV-2 induces acute neurological signs while Calcitonin Gene-Related Peptide (CGRP) signaling blockade reduces interleukin 6 (IL-6) release and weight loss in mouse models.

Shorter title: SARS-CoV-2 induces acute neurological signs while CGRP signaling blockade reduces interleukin 6 (IL-6) release and weight loss

Shafaqat.M. Rahman [1,co], David W. Buchholz[2,co], Brian Imbiakha.[2,co], Mason.C. Jager[3], Justin Leach, [1], Raven.M. Osborn [1], Ann O. Birmingham [1], Stephen Dewhurst[1], Hector C. Aguilar [2,*] , and Anne E. Luebke, [1,*]

[1]University of Rochester Medical Center, Departments of Biomedical Engineering, Neuroscience, Microbiology and Immunology, Rochester, NY, USA;

[2] Cornell University, Department of Microbiology and Immunology, College of Veterinary Medicine, Ithaca, NY, USA.

[3] Cornell University, Department of Population Medicine, College of Veterinary Medicine, Ithaca, NY, USA.

[co] Contributed equally

*Send correspondence to: Anne E. Luebke (aluebke@ur.rochester.edu) or Hector C. Aguilar (haguilar@cornell.edu)

Submitting author: Anne E. Luebke (aluebke@ur.rochester.edu)

Abstract:

COVID-19 can result in neurological symptoms such as fever, headache, dizziness, and nausea. We evaluated whether the Calcitonin Gene-Related Peptide (CGRP) receptor antagonist, olcegepant, used in migraine treatment could mitigate acute neuroinflammatory and neurological responses to SARS-COV-2 infection. We infected wildtype C57BL/6J and 129/SvEv mice, and a 129 αCGRP-null mouse line with a mouse-adapted SARS-CoV-2 virus, and evaluated the effect of CGRP receptor antagonism on the outcome of that infection. We determined that CGRP receptor antagonism provided protection from permanent weight loss in older (>12 m) C57BL/6J and 129 SvEv mice. We also observed acute fever and motion-induced dizziness in all older mice, regardless of treatment. However, in both wildtype mouse lines, CGRP antagonism reduced acute interleukin 6 (IL-6) levels by half, with virtually no IL-6 release in mice lacking αCGRP. These findings suggest that blockage of CGRP signaling protects against acute IL-6 release and subsequent inflammatory events after SARS-CoV-2 infection.

Introduction

Coronavirus disease (COVID-19) caused by severe acute respiratory syndrome CoV-2 (SARS-CoV-2) has caused a 3-year, ongoing, world pandemic [1]. There is a sound premise supporting testing CGRP-receptor antagonists such as olcegepant as a way to mitigate the neuroimmune consequences of SARS-CoV-2 infection [2]. While CGRP has pleotropic effects on the immune system, CGRP release occurs as a result of SARS-CoV-2 activation of the transient receptor potential (TRP) channels; and is implicated in COVID-19 neurological symptoms such as fever, headache, dizziness, nausea pain, and the subsequent release of interleukin 6 (IL-6) [3-5]. IL-6 is an important mediator of inflammation that is often elevated in severe COVID-19 infection, and may be involved in the hyperimmune response cascade (cytokine storm) and the polarization of T-cell responses [6, 7]. Headache, nausea, and dizziness are common neurological manifestations of COVID-19 infection [8, 9] and in COVID-19 patients headache severity has been correlated with IL-6 levels [10, 11].

Studies have shown that both SARS-CoV-1 (2002 outbreak) and SARS-CoV-2 (2019 outbreak) enter the body by binding to the angiotensin-converting enzyme 2 (ACE2) cell receptor [12, 13]. However, due to sequence and structural differences between mouse ACE2 and human ACE2, human SARS coronaviruses exhibit a species-restricted tropism and are inefficient at infecting wild-type mice. To overcome this obstacle, the Baric laboratory modified the clinical SARS-CoV-2/USA-WA1 variant to gain the ability to bind to the murine ACE2 receptor after serial passaging in mice, to generate the MA10-SARS-CoV-2 virus [14, 15]; we used this mouse-adapted virus in most of our study.

We first assessed both neurological symptoms of fever and dizziness/nausea in mouse models after infection with the MA10-SARS-CoV-2 virus. As a readout of the nausea-like state present after SARS-CoV-2 infection, we examined hypothermic responses to provocative motion, as we have previously used to assess migraine nausea pain (Biorxiv

66 doi.org/10.1101/2022.06.03.494762). Studies have demonstrated that provocative motion
67 causes robust and prominent hypothermic responses in rats, humans, house musk shrews, and
68 mice. These decreases in body temperature can represent a biomarker of a nausea-like state in
69 laboratory animals as: i) temperature changes are provoked both by motion and by chemical
70 emetic stimuli, ii) differential pharmacological sensitivity of these responses mirrors sensitivity in
71 humans, iii) motion-induced hypothermia *precedes* emetic (vomiting) episodes, and iv) there is a
72 clear parallel in hypothermic responses between animals and humans in underlying
73 physiological mechanism - cutaneous vasodilatation that favors heat loss [16-21]. In the
74 nausea/dizziness assay after provocative motion there is a decrease in head temperature and
75 an increase in tail temperature. We have shown that in wildtype C57BL/6Jmice injection of
76 Calcitonin Gene-Related Peptide (CGRP) prolongs this head temperature response and blunts
77 the transient tail temperature increase, whereas a CGRP-receptor antagonist can reverse these
78 CGRP-induced changes [22, 23] and Biorxiv doi.org/10.1101/2022.06.03.494762. Therefore,
79 we investigated if a MA10-SARS-CoV-2 viral infection would show similar acute
80 dizziness/nausea responses as CGRP injection, and if antagonizing CGRP signaling could
81 reduce these dizziness/nausea responses.
82

Results

MA-10 SARS-CoV-2 infection induces a fever-like state and disrupts thermoregulation to provocative motion. We measured baseline head temperatures in 18 month-old male /6J, 129SvEv, and 129 αCGRP-null groups of mice during pretesting and 3 days post-infection (dpi) with 10^5 pfu of MA-10 SARS-CoV-2 virus (**Fig. 2A&B**). Our results showed a higher head temperature at 3 dpi, indicating a fever in all mice, regardless of strain and olcegepant pretreatment (**Fig. 2B**).

We also measured motion-induced thermoregulation and weight changes in 18 month-old male C57BL/6J, 129SvEv, and 129 αCGRP-null groups of mice at 3 dpi with 10^5 pfu of MA-10 SARS-CoV-2 virus (**Fig. 3A**). Motion-induced thermoregulation was pre-tested in each mouse 5-7 days prior to the infection. During the pre-test, we observed transient tail vasodilation in response to provocative, nauseating stimuli (**Fig 3B,C,D**). The assay involved a 5-minute baseline recording, a 20-minute rotation period (75 rpm, 1 cm orbital displacement), and a 20-minute recovery period (as shown in **Figs. 1B and 3A**). Tail temperature profiles also indicated a fever-like state after infection with MA-10 SARS-CoV-2, with higher tail temperatures at all time points during the 3 dpi test than during the pretest (**Fig. 3B,C,D**). We computed a shift in the Δ tail vasodilations by subtracting the magnitude of Δ tail vasodilations at 3 dpi from an animal's pretest Δ tail vasodilation. With the exception of infected αCGRP-null mice, we observed a decrease in the magnitude of tail vasodilations in infected mice compared to their pretest, as indicated by a negative change in the Δ tail vasodilation - which is a sign of less severe dizziness.

Typically, a twenty-minute provocative rotation in mice causes observable hypothermia, and an additional 20-minute recovery period is needed for the mice to recover to their baseline head temperature. Interestingly, we observed that viral infection delayed this recovery period, as seen in our raw data (**Fig. 3 E,F,G**). Using a second-order polynomial fit ($B_0 + B_1X + B_2X^2$), we estimated the time required for the mice to recover back to their baseline head temperature by

109 interpolating a curve fit to t = 50 minutes (**Fig. 3H).** We then computed a Δ head recovery by
110 subtracting the recovery period at 3 dpi from the pretest, where a positive Δ head recovery
111 indicated a longer recovery period due to the infection. In all infected males, regardless of
112 olcegepant treatment or strain, we observed a longer recovery period at 3 dpi ($p < 0.0001$). No
113 protective effects were seen by olcegepant in head temperature recovery for either strain (**Fig.**
114 **3H**).

115

116 **Olcegepant blockage or developmental loss of CGRP receptor leads to reduced IL-6**
117 **production in response to MA-10 infection**

118 SARS-CoV-2 infected 129/SvEv mice treated with olcegepant pellets had lower
119 interleukin 6 (IL-6) concentrations in their bronchoalveolar lavage (BAL) as compared to mice
120 treated with placebo (**Fig. 4B**). Congruently, the lower IL-6 concentrations in olcegepant-treated
121 mice were similar to the IL-6 concentrations measured in the αCGRP-null (-/-) mice (**Fig 4B**),
122 which is consistent with the relationship between CGRP and IL-6 levels in migraines [24]. In
123 C57BL/6J mice, similar observations regarding olcegepant's effects in reducing IL-6 post-
124 infection were observed but did not reach statistical significance (**Fig 4A**).

125 **Older mice treated with olcegepant recovered from the initial weight loss by 7 dpi.**

126 When 18-month-old C57 or 129S mice were infected with MA-10, those pretreated with
127 olcegepant pellets showed a faster recovery to baseline weight compared to mice that received
128 placebo pellets. This effect was observed in both female and male C57BL/6J mice (**Fig. 5A**), as
129 well as in older female and male 129SvEv mice (**Fig. 5B**). Notably, 129S αCGRP (-/-) null mice
130 of either sex experienced similar trends as 129S WT mice given olcegepant (**Fig. 5E**). Older
131 infected mice exhibited lower core temperatures compared to the uninfected groups; however,
132 olcegepant had no distinguishable effect on core temperatures regardless of age or strain (**Fig.**
133 **5 B,D,F**). In addition, MA-10 infection did not significantly impact O_2% saturation in mice

134 regardless of age, sex, or strain. However αCGRP-null mice exhibited lower weight loss trends
135 following virus infection that did WT mice - suggesting that the αCGRP-null mice have a
136 reduced sensitivity to the MA-10 virus.

137 Histological analysis of lung tissue revealed no significant differences in the number of
138 SARS-CoV-2 infected cells in the lungs of C57BL/6J or 129S WT mice at 3 dpi (**Fig. 6 A&B**).
139 However, olcegepant-protected mice and αCGRP-null mice showed reduced staining for SARS-
140 CoV-2 when compared to placebo-treated mice, and this observation correlated with IL-6 levels.
141 **Fig. 6 C&D** shows SARS-CoV-2 staining (scale = 100 μm) of C57BL/6J (**C**) and 129S (**D**) lung
142 tissues.

143

144

145 **Discussion:**

146 Early in the pandemic, there was a controversy as to whether CGRP plasma levels were
147 increased or decreased in COVID-19 disease [25, 26]. However, a recent study with a relatively
148 greater number of patients showed that elevated CGRP plasma levels are correlated with
149 increased disease severity in hospitalized COVID-19 patients [27]. In our study, the migraine
150 drug olcegepant (small molecule CGRP receptor antagonist) reduced IL-6 release at three days
151 post-infection (3 dpi) in two distinct wildtype mouse strains (C57B6 and 129S). Interestingly
152 however, there was not a similar protective effect on fever or on the dizziness/nausea-like state
153 elicited by SARS-CoV-2 MA-10 in these same infected mice, as tested at 3 dpi.

154 A few studies have investigated CGRP antagonism on individuals infected with SARS-
155 CoV-2. In one study [28], no deleterious effects of CGRP antagonism were found, and no
156 differences in symptom severity were found between CGRP antagonism to other treatment
157 modalities in migraine subjects. However, in this study, patients were not stratified by age. We
158 observed CGRP antagonism was protective from weight loss and IL-6 release only in older
159 mice. COVID-19 symptoms are more severe and mortality rates are higher in aged human
160 patients, adding significance to our results. Further, two relatively recent case studies showed
161 that increased headaches after SARS-CoV-2 infection can be treated with CGRP monoclonal
162 antibodies [29, 30]. Our study suggests that olcegepant or other CGRP treatments may be
163 further explored particularly to treat headaches or migraines in aged individuals and/or those
164 with high IL-6 levels upon COVID-19 infection.

165 In conclusion, in addition to the acute effects studied here, antagonizing CGRP signaling
166 may be therapeutic against long COVID, as long COVID patients also show higher IL-6 plasma
167 levels [31]. As long COVID has been demonstrated in mouse models [32], future plans include
168 investigating if antagonizing CGRP signaling in preclinical models can mitigate neurological long
169 COVID symptoms.

170

Materials and Methods

Animals

A total of 180 mice (120 M/60F) were used in these studies, either 129SvEv (Taconic 129SVE) or C57B6/J (JAX 0664) or αCGRP (-/-) null mice on a 129SvEv background. Prior to SARS-CoV-2 infection, mice were bred and housed under a 12 to 12 day/night cycle at the University of Rochester 's Vivarium under the care of the University of Rochester's Veterinary Services personnel. Mice were implanted with transponder chips (Backagin Microchip FDX-B ISO 11784/11785) to allow for blinded identification; and when relevant, implanted with pellets containing placebo or olcegepant (BIBN4096, Tocris; 2 mg/kg/day/SQ; Innovative Research of America, Inc.). After pretesting was performed, mice were transferred to Cornell's ABSL3 facility, and acclimated prior to virus infection and testing. All animal procedures were approved both by the University of Rochester's and Cornell University's IACUC committees and performed in accordance with NIH standards.

Virus propagation

Vero-E6 cells (obtained through BEI resources, NIAID, NIH, NR-53726) were cultured in Eagle's Minimum Essential Medium (ATCC, #30-2003) supplemented with 10% (vol/vol) fetal bovine serum (FBS) (Gibco, CA) and 1% penicillin-streptomycin (Pen-Strep, Life Technologies) at 37°C in a 5% (vol/vol) CO_2 atmosphere. Viral stocks of mouse-adapted SARS-CoV-2 (MA10) (obtained from the laboratory Dr. Ralph Baric) were propagated in Vero-E6 cells in 2% (vol/vol) FBS and 1% penicillin-streptomycin at 37°C at a multiplicity of infection (MOI) of 0.1. Viral stock titers were determined by $TCID_{50}$ analysis. Viral propagation involving live SARS-CoV-2 was conducted in Biosafety level 3 (BSL3) facilities both at the University of Rochester and at Cornell University.

196 **Animal Biosafety level 3 (ABSL3) facility and viral inoculations**

197 Mice were anesthetized using isoflurane and subsequently intranasally infected with MA-
198 10 SARS-CoV-2. For infection with live virus, drops of the pre-characterized viral stock were
199 administered into the rostral meatus of the nose, with a total volume of 50 µL per mouse. Daily
200 monitoring and weighing of the mice were conducted until they reached a predetermined
201 humane endpoint of 20% weight loss from their starting weight and/or severe clinical signs, at
202 which point animals were humanely euthanized. Mouse studies were conducted in a BSL-3
203 laboratory and in accordance with protocols approved by the Institutional Animal Care and Use
204 Committee at Cornell University (IACUC mouse protocol # 2017-0108 and BSL3 IBC # MUA-
205 16371-1). See Fig. 1A.

206

207 **Motion-Induced Thermoregulation Testing**

208 Tu et al. first noticed thermoregulatory changes in the temperatures of the heads,
209 bodies, and tails of mice, in response to provocative motion [21] . We therefore adapted
210 their protocol for the present study (Biorxiv doi.org/10.1101/2022.06.03.494762). Head and
211 tail temperatures of C57B6/J mice were measured for a total of 45 minutes using a FLIR E60 IR
212 camera (model: E64501), as depicted in Fig. 1A. This camera was connected to a tripod and
213 positioned approximately 43 cm above an open, plexiglass box (mouse box) used to house an
214 individual mouse during testing. Both the tripod and mouse box were securely attached to the
215 shaker's base. Briefly, baseline measurements were recorded for five minutes prior to the
216 provocative motion (-5 to 0 mins). The provocative motion was an orbital rotation (75 rpm, 2-cm
217 orbital displacement), and mice were video-recorded for 20 minutes (0 to 20 mins). After 20
218 minutes, the provocative motion was turned off, and mice were video-recorded for an additional
219 20 minutes to measure recovery to baseline (20 to 40 mins) as schematized in Figs. 1A and 2.
220 Head and tail temperatures were measured after data retrieval using the software FLIR Tools+.
221 Tail and head temperatures were measured within predefined field of views: square region (3x3

222 mm) for tail, and circular region (10x10 mm) for head. Tail measurements occurred 2 cm from
223 the base of the tail and head measurements occurred at the center of the head image, in
224 between the mouse's ears. Infrared imaging data was collected every minute during baseline
225 measurements, and every 2 minutes during and after the provocative motion. We quantified
226 thermoregulatory changes to provocative motion by comparing changes in tail vasodilatations,
227 and we approximated the magnitude of the head hypothermia based on second order curve fit
228 estimates. Transient increases in the tail temperature of the mouse to provocative motion are
229 referred to as Δ *tail vasodilatations* (^{o}C), and were computed by subtracting the tail temperature
230 at time t = 0 minutes (rotation ON) from the max tail temperature measured during the first 10
231 mins of the rotation ($0 \leq t \leq 10$).

232

233 **Pulse Oximetry**

234 A mouse Stat Jr X (Kent Scientific) was used to measure oxygen saturation (O2%) of
235 mice (see Fig. 1B). The O_2 sensor was applied to the rear leg, and data were recorded following
236 readout stabilization, defined as an unchanging recording over 5 seconds.

237

238 **BAL harvest and tissue processing**

239 Mice were euthanized with CO_2 , and bronco-alveolar lavage BAL fluid was removed
240 from the lung; animals then underwent laparotomy and sternotomy with subsequent left and
241 right ventricular cardiac perfusion with 20 mL total of PBS. Lungs were treated with 4%
242 paraformaldehyde/PBS (volume/volume) for a minimum of 72 hours to ensure full viral
243 inactivation. Tissues were taken out of the BSL3 facility and underwent dehydration with ethanol
244 and were later embedded in paraffin blocks for histological analysis.

245

246 **Histopathology**

247 For histological examination, mouse lungs were collected directly after euthanasia and
248 placed in 10% neutral buffered formalin for 72 h, after which tissues were embedded in paraffin.
249 Four-micrometer tissue sections were stained with hematoxylin for analysis.
250 Immunohistochemistry and digital image analysis for SARS-CoV-2 nucleocapsid was performed
251 as previously described [33]. Briefly, 4 μm tissue sections were labeled with a rabbit IgG
252 monoclonal antibody against SARS-CoV-2 nucleocapsid protein (GeneTex; GTX635679) at a
253 1:5,000 dilution and processed using a Leica Bond Max automated IHC Stainer. Digital image
254 analysis was performed using QuPath software v.0.2.3 [33-36].

255

256 **Imaging**

257 Histological specimens were visualized using a Zeiss Axioplan 2 microscope.
258 Immunohistochemistry (IHC) and hematoxylin and eosin (HE) stained slides for each specimen
259 were photographed in sequential order. In Adobe Photoshop, all images were sized with a
260 2080x2080 pixel frame and cropped to a uniform resolution of 1500x1500 pixels. IHC images
261 were further analyzed using Color Selection and Magic Wand tools where areas containing
262 brown staining were manually selected and cut into a separate layer. All images were exported
263 into JPEG format. For staining percentages, quantification was performed using ImageJ.
264 Images were converted from RGB Color into 8-bit grayscale and made Binary to set an
265 automated threshold. Area was then calculated with the Analyze Particles function. Circularity of
266 staining was assessed using the Circularity parameter set to 0.9-1.0.

267 **Quantification of lavage cytokines by ELISA**

268 Immulux 4HBx plates (ThermoFisher Scientific, #3855) were coated with IL-6 capture
269 antibody (ThermoFisher Scientific, MP5-20F3) and left overnight at 4°C. Wells were washed five
270 times with PBS+0.05% Tween 20 and blocked with PBS+5% dry milk solution (Bio-Rad,

271 1706404) for 1 hour at room temperature. 50µL of lavage sample or standard (R&D systems,
272 406-ML-005/CF) was added to the blocked wells for 2 hours at room temperature. Bound
273 cytokine was detected using a biotinylated IL-6 detection antibody (ThermoFisher Scientific,
274 MP5-32C11), streptavidin horseradish peroxidase (strep-HRP), and tetramethylbenzidine (TMB)
275 (ThermoFisher Scientific, 34028). Wells were washed three times following the addition of
276 detection antibody and strep-HRP. Reactions were stopped with 2N H_2SO_4 and ODs were read
277 at 450nm. Cytokine concentrations for each sample were determined by plotting OD values on a
278 standard curve using IL-6 recombinant protein. All testing was performed in triplicate.

279

280 **Statistics**

281 Two-way mixed effects (ME) models were used to assess % weight loss, and core
282 temperatures (^{o}C) across the factors: i) placebo vs olcegepant protection and ii) dpi. Two-way
283 ME models were also used to assess: i) viral infection vs pretest and ii) placebo vs olcegepant
284 protection for tail vasodilation responses at 3 dpi. Bonferroni multiple comparisons test was the
285 preferred post-hoc analysis method. X-intercept analyses of head recovery (mins) were
286 conducted assuming a quadratic model, least squares regression fitting, and constraints where
287 the x-intercept must be greater than x = 20 mins and the curve fit was approximated to x = 50
288 mins. Nested 1-way ANOVAs with Tukey post hoc was used to analyze BAL IL-6
289 concentrations and H&E staining (positive SARS-CoV-2 cells per mm^2).

290

291 **Acknowledgments**

292 This research is supported by a COVID-19 research supplement to NIH R01 DC017261
293 (AEL). We would also like to thank Dr. Ralph S. Baric (UNC) for the MA-10 SARS CoV-2 virus
294 stock, the BSL3 facility and staff in the Center for Advanced Research Technologies at the
295 University of Rochester, and the ABSL3 facility and staff at Cornell University. We would also
296 like to thank Shruti Aryal for assisting with data analysis.

297

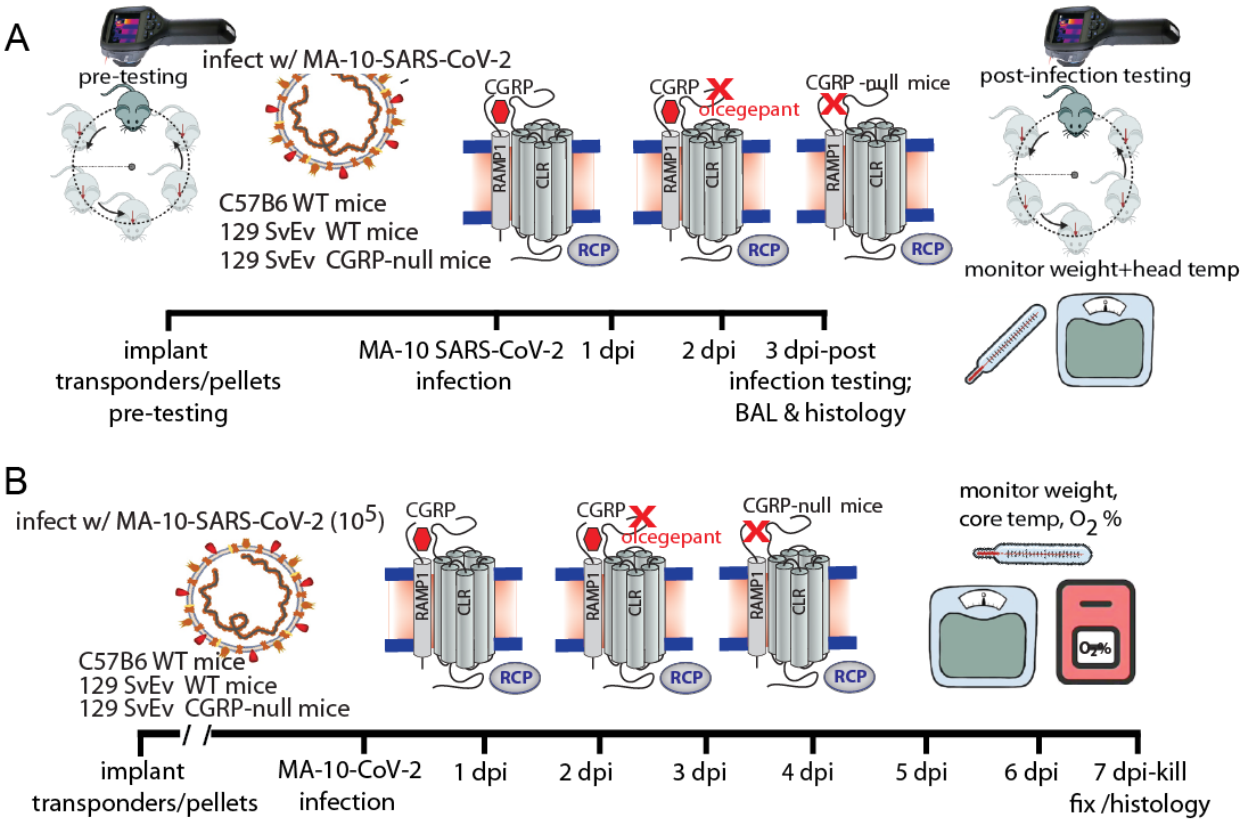

298

299 Fig. 1

300

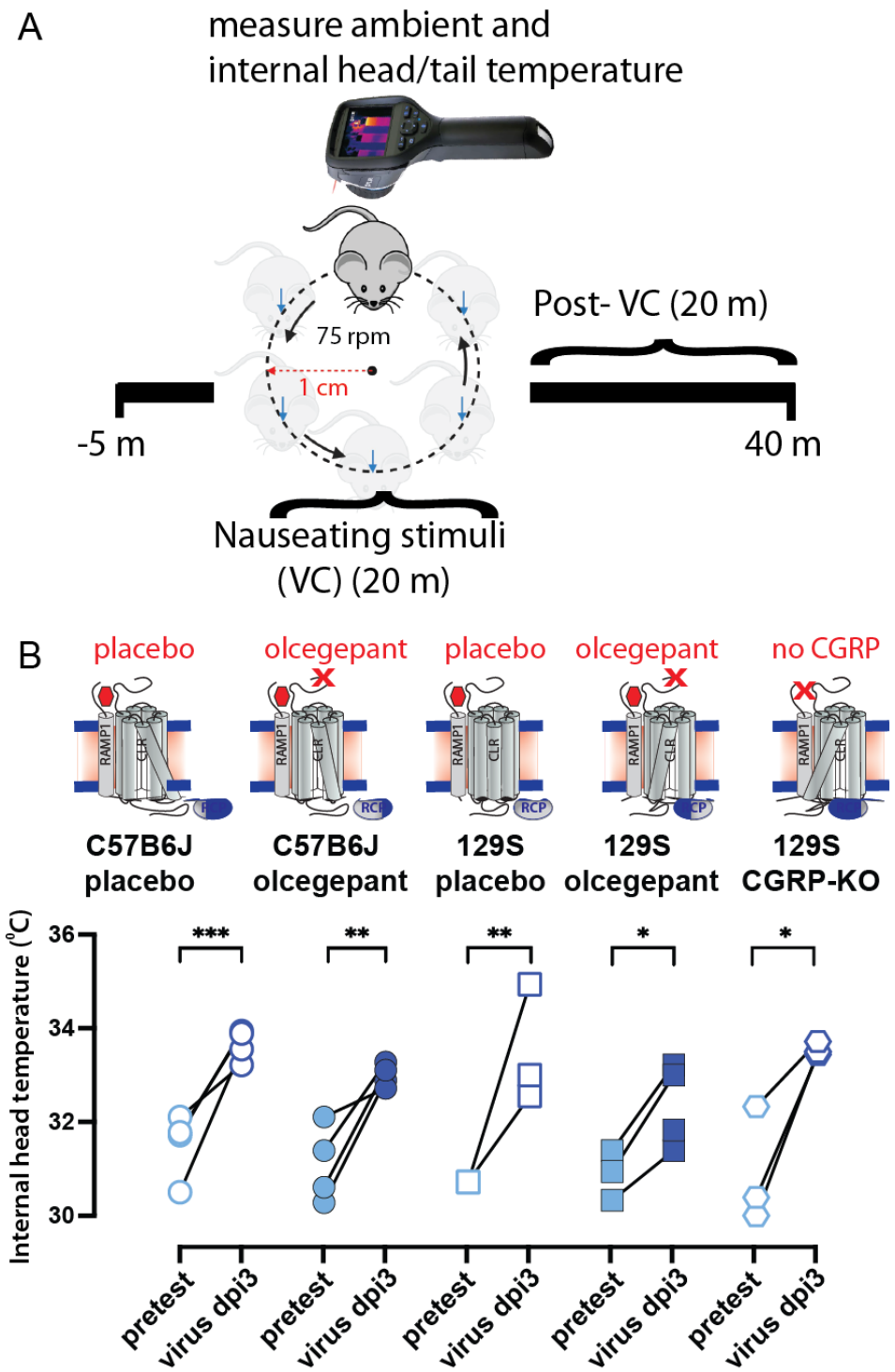
A
measure ambient and
internal head/tail temperature
75 rpm
1 cm
-5 m
Post- VC (20 m)
40 m
Nauseating stimuli
(VC) (20 m)
B
placebo
olcegepant
placebo
olcegepant
no CGRP
RAMP1
CLR
RCP
C57B6J
placebo
C57B6J
olcegepant
129S
placebo
129S
olcegepant
129S
CGRP-KO
Internal head temperature (°C)
36
34
32
30
***
**
**
*
*
pretest
virus dpi3

Fig. 2

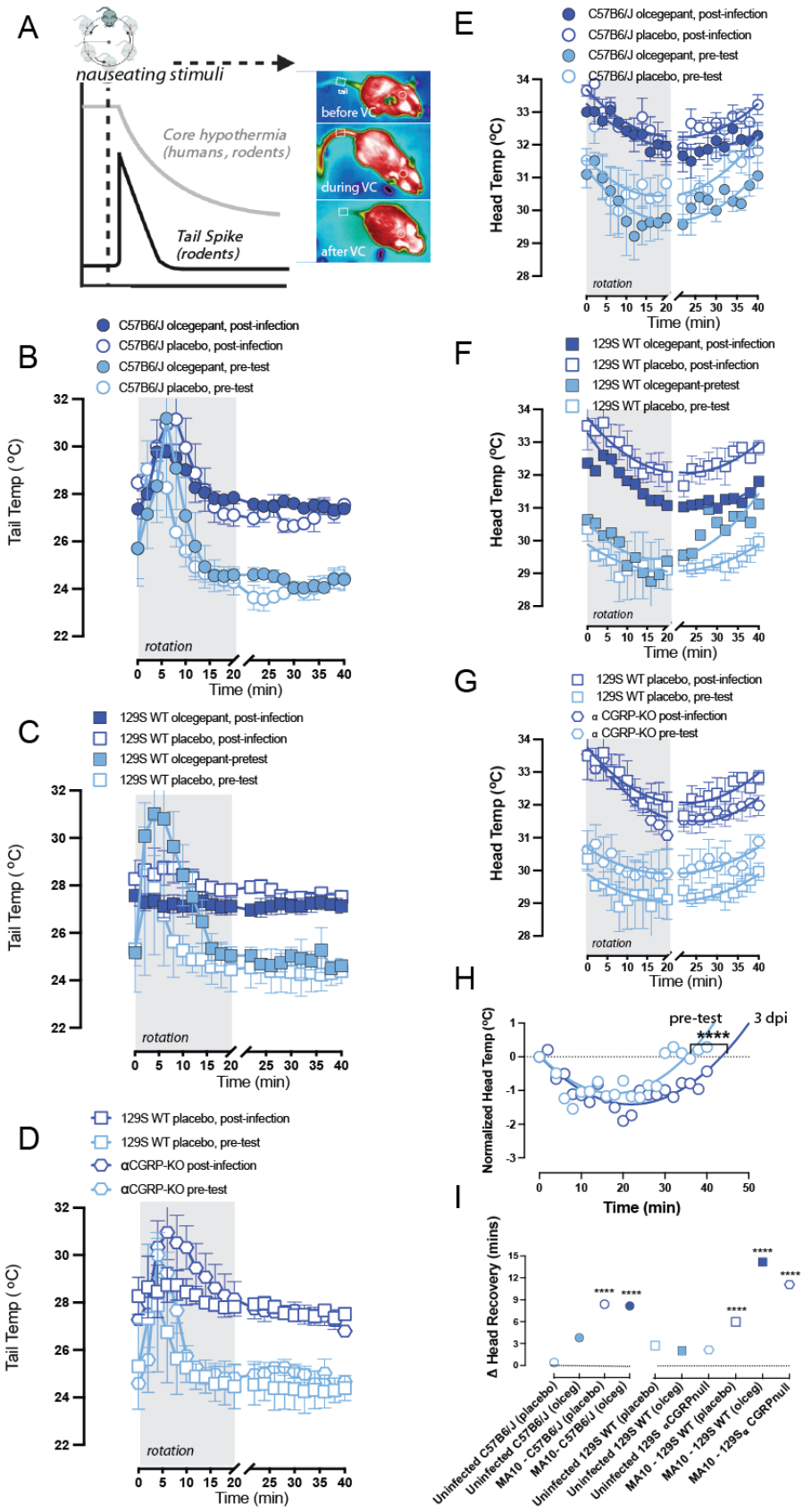
A
nauseating stimuli
Core hypothermia
(humans, rodents)
Tail Spike
(rodents)
before VC
during VC
after VC
B
C57B6/J olcegepant, post-infection
C57B6/J placebo, post-infection
C57B6/J olcegepant, pre-test
C57B6/J placebo, pre-test
Tail Temp (°C)
rotation
Time (min)
C
129S WT olcegepant, post-infection
129S WT placebo, post-infection
129S WT olcegepant-pretest
129S WT placebo, pre-test
Tail Temp (°C)
rotation
Time (min)
D
129S WT placebo, post-infection
129S WT placebo, pre-test
αCGRP-KO post-infection
αCGRP-KO pre-test
Tail Temp (°C)
rotation
Time (min)
E
C57B6/J olcegepant, post-infection
C57B6/J placebo, post-infection
C57B6/J olcegepant, pre-test
C57B6/J placebo, pre-test
Head Temp (°C)
rotation
Time (min)
F
129S WT olcegepant, post-infection
129S WT placebo, post-infection
129S WT olcegepant-pretest
129S WT placebo, pre-test
Head Temp (°C)
rotation
Time (min)
G
129S WT placebo, post-infection
129S WT placebo, pre-test
α CGRP-KO post-infection
α CGRP-KO pre-test
Head Temp (°C)
rotation
Time (min)
H
pre-test
3 dpi
****
Normalized Head Temp (°C)
Time (min)
I
Δ Head Recovery (mins)
Uninfected C57B6/J (placebo)
Uninfected C57B6/J (olceg)
MA10 - C57B6/J (placebo)
MA10- C57B6/J (olceg)
Uninfected 129S WT (placebo)
Uninfected 129S WT (olceg)
Uninfected 129S αCGRPnull
MA10 - 129S WT (placebo)
MA10 - 129S WT (olceg)
MA10 - 129Sα CGRPnull

Fig. 3

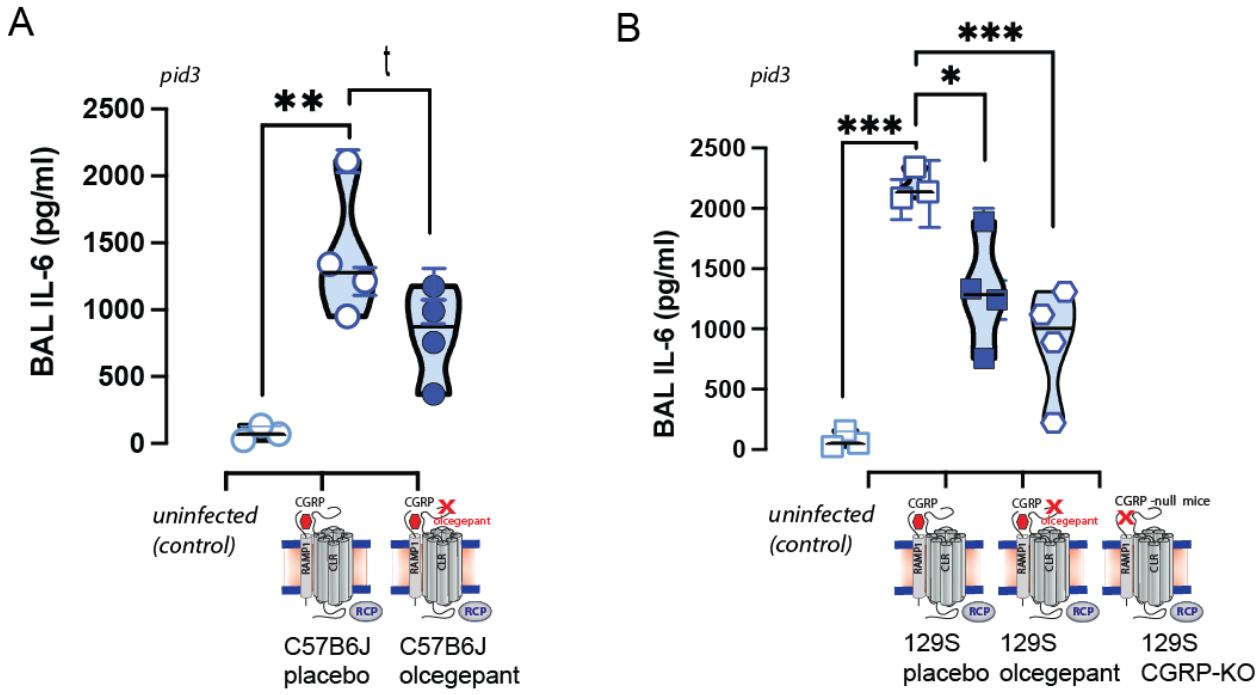
A
pid3
BAL IL-6 (pg/ml)
2500
2000
1500
1000
500
0
**
t
uninfected
(control)
CGRP
RAMP1
CLR
RCP
olcegepant
C57B6J
placebo
C57B6J
olcegepant
B
pid3
***
*
***
BAL IL-6 (pg/ml)
2500
2000
1500
1000
500
0
uninfected
(control)
CGRP
RAMP1
CLR
RCP
olcegepant
CGRP -null mice
129S
placebo
129S
olcegepant
129S
CGRP-KO

Fig. 4

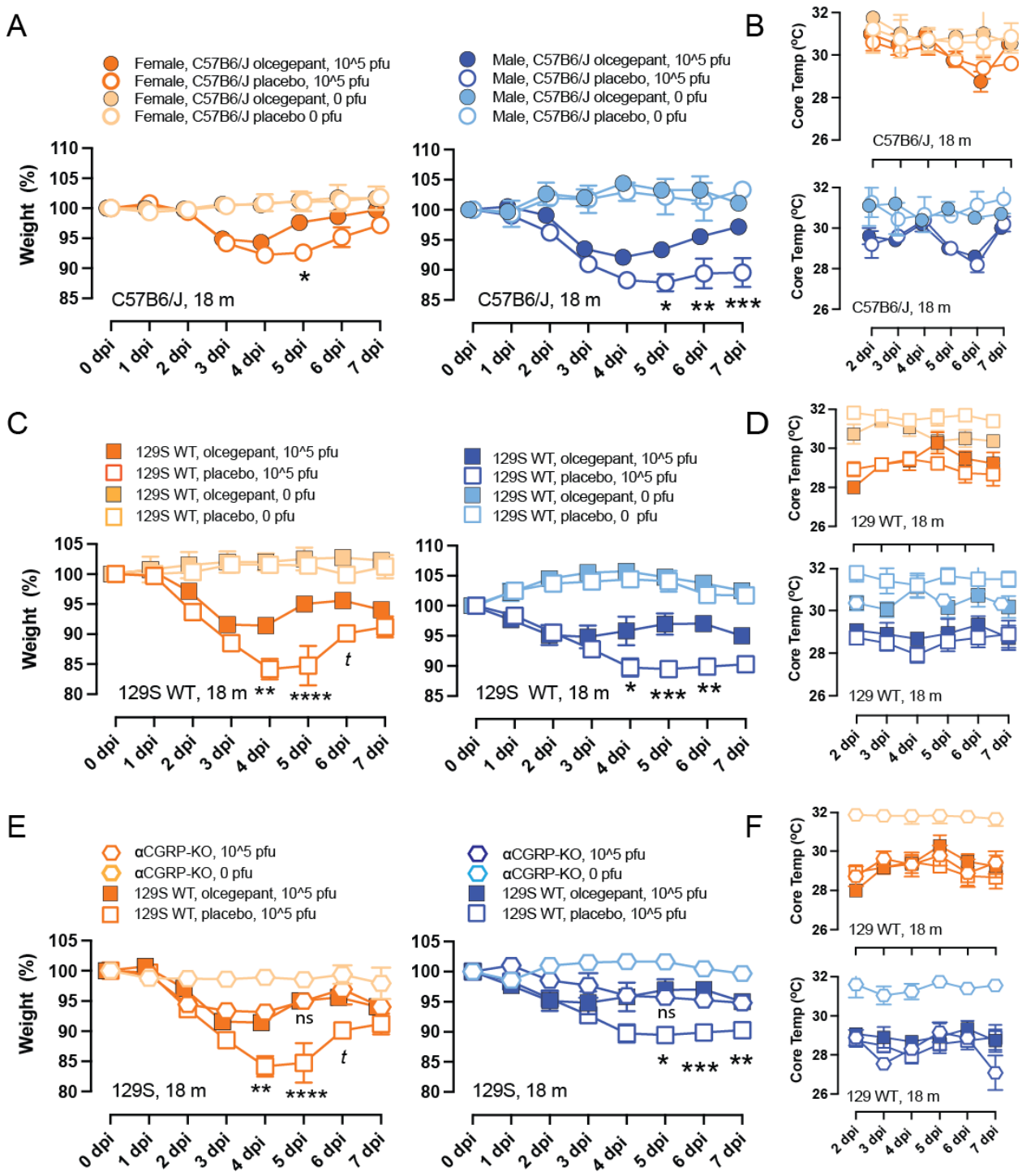
A
Female, C57B6/J olcegepant, 10^5 pfu
Female, C57B6/J placebo, 10^5 pfu
Female, C57B6/J olcegepant, 0 pfu
Female, C57B6/J placebo 0 pfu
Male, C57B6/J olcegepant, 10^5 pfu
Male, C57B6/J placebo, 10^5 pfu
Male, C57B6/J olcegepant, 0 pfu
Male, C57B6/J placebo, 0 pfu
Weight (%)
C57B6/J, 18 m
B
Core Temp (°C)
C57B6/J, 18 m
C
129S WT, olcegepant, 10^5 pfu
129S WT, placebo, 10^5 pfu
129S WT, olcegepant, 0 pfu
129S WT, placebo, 0 pfu
129S WT, 18 m
D
129 WT, 18 m
E
αCGRP-KO, 10^5 pfu
αCGRP-KO, 0 pfu
129S WT, olcegepant, 10^5 pfu
129S WT, placebo, 10^5 pfu
129S, 18 m
ns
F
0 dpi
1 dpi
2 dpi
3 dpi
4 dpi
5 dpi
6 dpi
7 dpi

Fig. 5

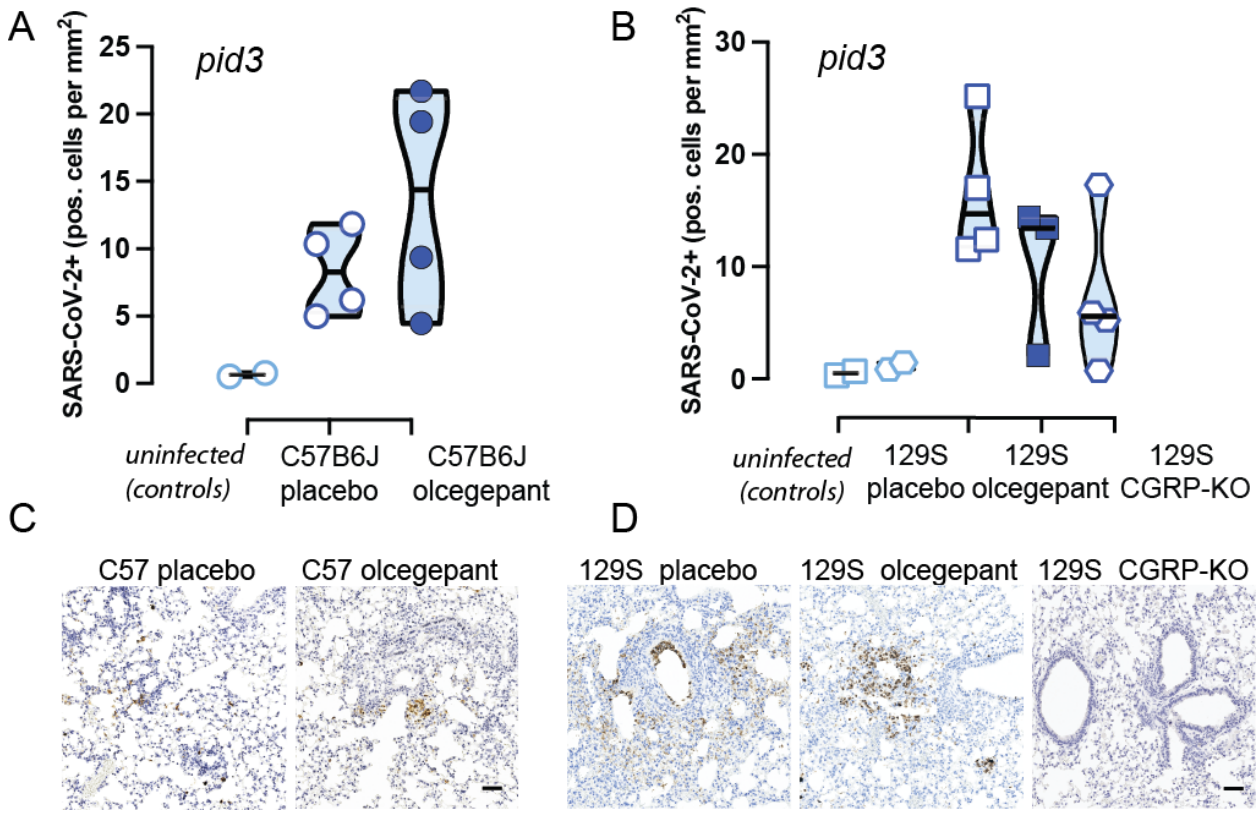
A
pid3
SARS-CoV-2+ (pos. cells per mm²)
25
20
15
10
5
0
uninfected (controls)
C57B6J placebo
C57B6J olcegepant
B
pid3
SARS-CoV-2+ (pos. cells per mm²)
30
20
10
0
uninfected (controls)
129S placebo
129S olcegepant
129S CGRP-KO
C
C57 placebo
C57 olcegepant
D
129S placebo
129S olcegepant
129S CGRP-KO

Fig. 6

330 **Figure Legends:**

331 **Fig. 1.** The study timelines are depicted. **A.** WT mice were infected with 10^5 pfu of MA-10
332 SARS-CoV-2 in the presence of placebo or CGRP-receptor antagonist olcegepant slow-release
333 pellets (olcegepant, BIBN4096, Tocris; 2 mg/kg/day/SQ) or mice lacking CGRP were infected
334 with the same virus; animals were then assessed for motion-induced nausea (dizziness) at 3
335 days after viral infection (dpi). At the completion of the nausea testing at 3dpi, bronchoalveolar
336 lavage (BAL) samples were collected for ELISA and lung tissue was obtained from control and
337 virus-infected animals at 3 dpi. Nausea (dizziness) was assessed for 45 minutes when mouse
338 was subjected to an orbital motion, noting temperature profiles (head and tail). **B.** WT mice
339 were infected with 10^5 pfu of MA-10 SARS-CoV-2 in the presence of placebo or CGRP-receptor
340 antagonist olcegepant slow-release pellets (olcegepant, BIBN4096, Tocris; 2 mg/kg/day/SQ) or
341 mice lacking CGRP were infected with the same virus; animals were then monitored for
342 changed in weight, core temperature and oxygen (O_2) saturation from 0 to 7 dpi.

343

344 **Fig. 2.** As shown in the **Fig 1A** timeline, older C57B/6, 129SvEv, and 129 mice lacking CGRP
345 were assessed for nausea (dizziness) when subjected to an orbital rotation, noting temperature
346 profiles (head and tail). **A.** Head and tail temperatures of mice were measured for a total 45
347 minutes using a FLIR E60 IR camera (model: E64501). This camera was connected to a tripod
348 and positioned approximately 43 cm above an open, plexiglass box (mouse box) used to house
349 an individual mouse during testing. Both the tripod and mouse box are securely attached to the
350 shaker's base. Briefly, baseline measurements were recorded for five minutes prior to the
351 provocative motion (-5 to 0 mins). The provocative motion was an orbital rotation (75 rpm, 2-cm
352 orbital displacement), and mice were recorded for 20 minutes (0 to 20 mins). After 20 minutes,
353 the provocative motion was turned off, and mice were recorded for an additional 20 minutes to
354 measure recovery to baseline (20 to 40 mins). Three mouse strains were tested: C57/B6J WT,
355 129S WT, and 129S αCGRP-null mice. Within each wild type (WT) strain, four groups of mice
356 were tested: placebo only, olcegepant only, placebo with 10^5 MA-SARS-CoV-2, and olcegepant

357 with 10^5 SARS-CoV-2 MA-10. Virus-infected mice were tested at Cornell University's ABSL-3
358 environment, with all pre-infection testing performed at University of Rochester. **B.** All tested
359 mice experienced a fever-like state 3 days post-viral infection (3 dpi). Olcegepant did not have a
360 protective effect in reducing this acute fever-like state at 3 dpi.

361

362 **Fig. 3. A.** Upon provocative motion, humans and mice will show a drop in head temperature
363 that recovers once rotation is ceased, and mice show a transient tail spike ~10 min into rotation.
364 When nausea or dizziness is present, the head temperature drop takes longer to recover, and
365 the transient tail spike diminishes or disappears. **B,C,D.** Viral infection diminishes tail
366 vasodilatations and impairs a mouse's natural response to the provocative motion. At time t = 0,
367 mice experience a 20-minute provocative motion and exhibit a significant increase in tail
368 temperature. Δ tails are computed and are corrected for ambient temperature. Findings suggest
369 that olcegepant did not protect against virus-induced changes in tail vasodilation at 3 dpi in all of
370 the strains tested. **E,F,G.** Viral infection impacts recovery from hypothermia after provocative
371 motion. **H.** Second order curve fits observed recovery of head temperatures after provocative
372 motion to baseline. Across all strains, mice experienced delayed temperature recovery
373 compared to pretest, with longer recovery profiles. **I.** No protective effects were seen by
374 olcegepant in temperature recovery for any of the tested strains.

375

376

377 **Fig. 4.** Bronco-alveolar lavage (BAL) samples were obtained for ELISA testing, and lungs were
378 obtained for subsequent immunohistochemistry at 3 dpi. MA-SARS-CoV-2 infection increased
379 the release of the inflammatory cytokine IL-6, and this IL-6 release was attenuated by CGRP
380 signaling blockade. In both C57B6/J **(A)** and 129S mice **(B)** strains, IL-6 release was
381 attenuated by olcegepant SQ release. Moreover, in αCGRP null mice, IL-6 cytokine release was
382 statistically equivalent to non-infected controls **(B)**.

383

384 **Fig. 5.** Older (18 months) female and male mice were tested for weight loss and core
385 temperature drops after infection with MA-10 SARS-CoV-2, 10^5 pfu virus at 0-7 dpi. **A. C.** We
386 found that animals treated with olcegepant recovered from the initial weight loss, with male mice
387 showing increased protection. **A.** C57B6/J; **C.** 129S. **E.** Similar to the IL-6 findings (**Fig. 4**),
388 mice lacking the CGRP peptide were not significantly different from uninfected controls. **B, D,**
389 **F.** Viral infection caused core temperatures of mice to decrease, and this effect was unaltered
390 by olcegepant treatment.

391

392 **Fig. 6.** A**&B.** There was no statistically significant difference in the number of SARS-CoV-2
393 antigen-positive cells in the lungs of (**A, C**) C57/B6J or (**B, D**) 129 mice, between mice that
394 received placebo versus olcegepant pellets at 3 dpi. **C, D.** Representative SARS-CoV-2
395 immunostaining is shown for 3 dpi lung issues from C57B6/J (**C**), and 129S (**D**) mice. Scale bar
396 is 100 μm. (*= $p < 0.05$, ** =$p < 0.01$, ** *= $p < 0.001$, **** = $p < 0.0001$)

397

398 **References:**

399 1. Zhu N, Zhang D, Wang W, Li X, Yang B, Song J, et al. A Novel Coronavirus from
400 Patients with Pneumonia in China, 2019. N Engl J Med. 2020;382(8):727-33. Epub 2020/01/25.
401 doi: 10.1056/NEJMoa2001017. PubMed PMID: 31978945; PubMed Central PMCID:
402 PMCPMC7092803.

403 2. Robertson CE. Could CGRP antagonists be helpful in the fight against COVID-19?
404 Headache. 2020. Epub 2020/05/10. doi: 10.1111/head.13853. PubMed PMID: 32386433.

405 3. Assas BM, Miyan JA, Pennock JL. Cross-talk between neural and immune receptors
406 provides a potential mechanism of homeostatic regulation in the gut mucosa. Mucosal Immunol.
407 2014;7(6):1283-9. Epub 2014/09/04. doi: 10.1038/mi.2014.80. PubMed PMID: 25183366.

408 4. Assas BM, Pennock JI, Miyan JA. Calcitonin gene-related peptide is a key
409 neurotransmitter in the neuro-immune axis. Front Neurosci. 2014;8:23. Epub 2014/03/05. doi:
410 10.3389/fnins.2014.00023. PubMed PMID: 24592205; PubMed Central PMCID:
411 PMCPMC3924554.

412 5. Channappanavar R, Perlman S. Pathogenic human coronavirus infections: causes and
413 consequences of cytokine storm and immunopathology. Semin Immunopathol. 2017;39(5):529-
414 39. Epub 2017/05/04. doi: 10.1007/s00281-017-0629-x. PubMed PMID: 28466096; PubMed
415 Central PMCID: PMCPMC7079893.

416 6. Aghagoli G, Gallo Marin B, Katchur NJ, Chaves-Sell F, Asaad WF, Murphy SA.
417 Neurological Involvement in COVID-19 and Potential Mechanisms: A Review. Neurocrit Care.
418 2021;34(3):1062-71. Epub 2020/07/15. doi: 10.1007/s12028-020-01049-4. PubMed PMID:
419 32661794; PubMed Central PMCID: PMCPMC7358290.

420 7. Liu Y, Zhang C, Huang F, Yang Y, Wang F, Yuan J, et al. Elevated plasma levels of
421 selective cytokines in COVID-19 patients reflect viral load and lung injury. Natl Sci Rev.

422 2020;7(6):1003-11. Epub 2020/06/01. doi: 10.1093/nsr/nwaa037. PubMed PMID: 34676126;
423 PubMed Central PMCID: PMCPMC7107806.

424 8. Bohn MK, Hall A, Sepiashvili L, Jung B, Steele S, Adeli K. Pathophysiology of COVID-
425 19: Mechanisms Underlying Disease Severity and Progression. Physiology (Bethesda).
426 2020;35(5):288-301. Epub 2020/08/14. doi: 10.1152/physiol.00019.2020. PubMed PMID:
427 32783610; PubMed Central PMCID: PMCPMC7426542.

428 9. Saniasiaya J, Kulasegarah J. Dizziness and COVID-19. Ear Nose Throat J.
429 2021;100(1):29-30. Epub 2020/09/16. doi: 10.1177/0145561320959573. PubMed PMID:
430 32931322; PubMed Central PMCID: PMCPMC7492824.

431 10. Bolay H, Karadas O, Ozturk B, Sonkaya R, Tasdelen B, Bulut TDS, et al. HMGB1,
432 NLRP3, IL-6 and ACE2 levels are elevated in COVID-19 with headache: a window to the
433 infection-related headache mechanism. J Headache Pain. 2021;22(1):94. Epub 2021/08/14. doi:
434 10.1186/s10194-021-01306-7. PubMed PMID: 34384355; PubMed Central PMCID:
435 PMCPMC8358545.

436 11. Karadas O, Ozturk B, Sonkaya AR, Tasdelen B, Ozge A, Bolay H. Latent class cluster
437 analysis identified hidden headache phenotypes in COVID-19: impact of pulmonary infiltration
438 and IL-6. Neurol Sci. 2021;42(5):1665-73. Epub 2021/02/10. doi: 10.1007/s10072-020-04978-2.
439 PubMed PMID: 33559789; PubMed Central PMCID: PMCPMC7870778.

440 12. Kuba K, Imai Y, Rao S, Gao H, Guo F, Guan B, et al. A crucial role of angiotensin
441 converting enzyme 2 (ACE2) in SARS coronavirus-induced lung injury. Nat Med.
442 2005;11(8):875-9. Epub 2005/07/12. doi: 10.1038/nm1267. PubMed PMID: 16007097; PubMed
443 Central PMCID: PMCPMC7095783.

444 13. Ziegler CGK, Allon SJ, Nyquist SK, Mbano IM, Miao VN, Tzouanas CN, et al. SARS-
445 CoV-2 Receptor ACE2 Is an Interferon-Stimulated Gene in Human Airway Epithelial Cells and Is

446 Detected in Specific Cell Subsets across Tissues. Cell. 2020. Epub 2020/05/16. doi:
447 10.1016/j.cell.2020.04.035. PubMed PMID: 32413319.

448 14. Dinnon KH, 3rd, Leist SR, Schafer A, Edwards CE, Martinez DR, Montgomery SA, et al.
449 A mouse-adapted model of SARS-CoV-2 to test COVID-19 countermeasures. Nature.
450 2020;586(7830):560-6. Epub 2020/08/28. doi: 10.1038/s41586-020-2708-8. PubMed PMID:
451 32854108; PubMed Central PMCID: PMCPMC8034761.

452 15. Dinnon KH, 3rd, Leist SR, Schafer A, Edwards CE, Martinez DR, Montgomery SA, et al.
453 Publisher Correction: A mouse-adapted model of SARS-CoV-2 to test COVID-19
454 countermeasures. Nature. 2021;590(7844):E22. Epub 2021/01/21. doi: 10.1038/s41586-020-
455 03107-5. PubMed PMID: 33469219.

456 16. Del Vecchio F, Nalivaiko E, Cerri M, Luppi M, Amici R. Provocative motion causes fall in
457 brain temperature and affects sleep in rats. Exp Brain Res. 2014;232(8):2591-9. doi:
458 10.1007/s00221-014-3899-8. PubMed PMID: 24658633.

459 17. Mazloumi Gavgani A, Hodgson DM, Nalivaiko E. Effects of visual flow direction on signs
460 and symptoms of cybersickness. PLoS One. 2017;12(8):e0182790. doi:
461 10.1371/journal.pone.0182790. PubMed PMID: 28777827; PubMed Central PMCID:
462 PMCPMC5544223.

463 18. Nalivaiko E, Rudd JA, So RH. Motion sickness, nausea and thermoregulation: The
464 "toxic" hypothesis. Temperature (Austin). 2014;1(3):164-71. doi:
465 10.4161/23328940.2014.982047. PubMed PMID: 27626043; PubMed Central PMCID:
466 PMCPMC5008705.

467 19. Ngampramuan S, Cerri M, Del Vecchio F, Corrigan JJ, Kamphee A, Dragic AS, et al.
468 Thermoregulatory correlates of nausea in rats and musk shrews. Oncotarget. 2014;5(6):1565-

469 75. doi: 10.18632/oncotarget.1732. PubMed PMID: 24728971; PubMed Central PMCID:
470 PMCPMC4039232.

471 20. Romano F, Caramia N, Straumann D, Nalivaiko E, Bertolini G. Cross-coupling vestibular
472 stimulation: motion sickness and the vestibulo-sympathetic reflex. J Neurol. 2017. doi:
473 10.1007/s00415-017-8496-x. PubMed PMID: 28455665.

474 21. Tu L, Poppi L, Rudd J, Cresswell ET, Smith DW, Brichta A, et al. Alpha-9 nicotinic
475 acetylcholine receptors mediate hypothermic responses elicited by provocative motion in mice.
476 Physiol Behav. 2017;174:114-9. doi: 10.1016/j.physbeh.2017.03.012. PubMed PMID:
477 28302571.

478 22. Doods H, Hallermayer G, Wu D, Entzeroth M, Rudolf K, Engel W, et al. Pharmacological
479 profile of BIBN4096BS, the first selective small molecule CGRP antagonist. Br J Pharmacol.
480 2000;129(3):420-3. Epub 2000/03/11. doi: 10.1038/sj.bjp.0703110. PubMed PMID: 10711339;
481 PubMed Central PMCID: PMCPMC1571877.

482 23. Mallee JJ, Salvatore CA, LeBourdelles B, Oliver KR, Longmore J, Koblan KS, et al.
483 Receptor activity-modifying protein 1 determines the species selectivity of non-peptide CGRP
484 receptor antagonists. J Biol Chem. 2002;277(16):14294-8. Epub 2002/02/16. doi:
485 10.1074/jbc.M109661200. PubMed PMID: 11847213.

486 24. Han D. Association of Serum Levels of Calcitonin Gene-related Peptide and Cytokines
487 during Migraine Attacks. Ann Indian Acad Neurol. 2019;22(3):277-81. Epub 2019/07/31. doi:
488 10.4103/aian.AIAN_371_18. PubMed PMID: 31359937; PubMed Central PMCID:
489 PMCPMC6613407.

490 25. Abobaker A, Darrat M. Letter to the Editor From Abobaker and Darrat: "Circulating
491 Levels of Calcitonin Gene-Related Peptide Are Lower in COVID-19 Patients". J Endocr Soc.

492 2021;5(10):bvab052. Epub 2021/08/17. doi: 10.1210/jendso/bvab052. PubMed PMID:
493 34396020; PubMed Central PMCID: PMCPMC8083661.

494 26. Ochoa-Callejero L, Garcia-Sanmartin J, Villoslada-Blanco P, Iniguez M, Perez-Matute P,
495 Pujadas E, et al. Response to Letter to the Editor from Abobaker and Darrat: "Circulating levels
496 of Calcitonin Gene-Related Peptide Are Lower in COVID-19 Patients". J Endocr Soc.
497 2021;5(10):bvab053. Epub 2021/08/17. doi: 10.1210/jendso/bvab053. PubMed PMID:
498 34396021; PubMed Central PMCID: PMCPMC8083267.

499 27. Rizzi M, Tonello S, Morani F, Rizzi E, Casciaro GF, Matino E, et al. CGRP Plasma
500 Levels Correlate with the Clinical Evolution and Prognosis of Hospitalized Acute COVID-19
501 Patients. Viruses. 2022;14(10). Epub 2022/10/28. doi: 10.3390/v14102123. PubMed PMID:
502 36298678; PubMed Central PMCID: PMCPMC9611580.

503 28. Caronna E, Jose Gallardo V, Alpuente A, Torres-Ferrus M, Sanchez-Mateo NM,
504 Viguera-Romero J, et al. Safety of anti-CGRP monoclonal antibodies in patients with migraine
505 during the COVID-19 pandemic: Present and future implications. Neurologia (Engl Ed).
506 2021;36(8):611-7. Epub 2021/10/17. doi: 10.1016/j.nrleng.2021.03.005. PubMed PMID:
507 34654536; PubMed Central PMCID: PMCPMC8506139.

508 29. Grassini A, Marcinno A, Roveta F, Gallo E, Cermelli A, Boschi S, et al. Impact of COVID-
509 19 on chronic migraine treated with erenumab: a case report. Neurol Sci. 2021;42(8):3079-81.
510 Epub 2021/05/23. doi: 10.1007/s10072-021-05329-5. PubMed PMID: 34021438; PubMed
511 Central PMCID: PMCPMC8139216.

512 30. Ozkan E, Celebi O, Keskin O, Gursoy A, Gursoy-Ozdemir Y. Is Persistent Post-COVID
513 Headache Associated With Protein-Protein Interactions Between Antibodies Against Viral Spike
514 Protein and CGRP Receptor?: A Case Report. Front Pain Res (Lausanne). 2022;3:858709.

515 Epub 2022/04/19. doi: 10.3389/fpain.2022.858709. PubMed PMID: 35434707; PubMed Central
516 PMCID: PMCPMC9011137.

517 31. Littlefield KM, Watson RO, Schneider JM, Neff CP, Yamada E, Zhang M, et al. SARS-
518 CoV-2-specific T cells associate with inflammation and reduced lung function in pulmonary post-
519 acute sequalae of SARS-CoV-2. PLoS Pathog. 2022;18(5):e1010359. Epub 2022/05/27. doi:
520 10.1371/journal.ppat.1010359. PubMed PMID: 35617421; PubMed Central PMCID:
521 PMCPMC9176759.

522 32. Dinnon KH, Leist SR, Okuda K, Dang H, Fritch EJ, Gully KL, et al. A model of persistent
523 post SARS-CoV-2 induced lung disease for target identification and testing of therapeutic
524 strategies. bioRxiv. 2022. Epub 2022/02/24. doi: 10.1101/2022.02.15.480515. PubMed PMID:
525 35194605; PubMed Central PMCID: PMCPMC8863140.

526 33. Shapira T, Monreal IA, Dion SP, Buchholz DW, Imbiakha B, Olmstead AD, et al.
527 A TMPRSS2 inhibitor acts as a pan-SARS-CoV-2 prophylactic and therapeutic. Nature.
528 2022;605(7909):340-8. Epub 2022/03/29. doi: 10.1038/s41586-022-04661-w. PubMed PMID:
529 35344983; PubMed Central PMCID: PMCPMC9095466 US10988505B2) that cover matriptase
530 and other type II transmembrane serine proteases inhibitors for treating and preventing viral
531 infections, respiratory disorders, inflammatory disorders, pain disorders, tissue disorders,
532 hyperproliferative disorders, and disorders associated with iron overload. The remaining authors
533 declare that they have no competing interests.

534 34. Achanta R, Shaji A, Smith K, Lucchi A, Fua P, Susstrunk S. SLIC superpixels compared
535 to state-of-the-art superpixel methods. IEEE Trans Pattern Anal Mach Intell. 2012;34(11):2274-
536 82. Epub 2012/05/30. doi: 10.1109/TPAMI.2012.120. PubMed PMID: 22641706.

537 35. Bankhead P, Loughrey MB, Fernandez JA, Dombrowski Y, McArt DG, Dunne PD, et al.
538 QuPath: Open source software for digital pathology image analysis. Sci Rep. 2017;7(1):16878.

539 Epub 2017/12/06. doi: 10.1038/s41598-017-17204-5. PubMed PMID: 29203879; PubMed
540 Central PMCID: PMCPMC5715110.

541 36. Shapira T, Monreal IA, Dion SP, Jager M, Desilets A, Olmstead AD, et al. A novel highly
542 potent inhibitor of TMPRSS2-like proteases blocks SARS-CoV-2 variants of concern and is
543 broadly protective against infection and mortality in mice. bioRxiv. 2021. Epub 2021/05/12. doi:
544 10.1101/2021.05.03.442520. PubMed PMID: 33972944; PubMed Central PMCID:
545 PMCPMC8109206.

546